frontiers | Frontiers in Earth Science

TYPE Original Research
PUBLISHED 16 November 2023
DOI 10.3389/feart.2023.1307303

OPEN ACCESS

EDITED BY
Yong Wang,
Southwest Petroleum University, China

REVIEWED BY
Tomoaki Morishita,
Kanazawa University, Japan
Karoly Nemeth,
Institute of Earth Physics and Space Sciences, Hungary
Ian Ernest Masterman Smith,
The University of Auckland, New Zealand

*CORRESPONDENCE
Anastassia Y. Borisova,
anastassia.borisova@get.omp.eu

RECEIVED 04 October 2023
ACCEPTED 23 October 2023
PUBLISHED 16 November 2023

CITATION
Borisova AY, Melnik OE, Gaborit N, Bindeman IN, Traillou T, Raffarin M, Stefánsson A, Laurent O, Leisen M, Llovet X, de Parseval P, Proietti A and Tait S (2023), *In situ* probing of the present-day zircon-bearing magma chamber at Krafla, Northeastern Iceland. *Front. Earth Sci.* 11:1307303. doi: 10.3389/feart.2023.1307303

In situ probing of the present-day zircon-bearing magma chamber at Krafla, Northeastern Iceland

Anastassia Y. Borisova[1]*, Oleg E. Melnik[1,2], Nicolas Gaborit[1], Ilya N. Bindeman[3], Thibault Traillou[1], Marie Raffarin[1], Andri Stefánsson[4], Oscar Laurent[1], Mathieu Leisen[1], Xavier Llovet[5], Philippe de Parseval[1], Arnaud Proietti[6] and Stephen Tait[1]

[1]Géosciences Environnement Toulouse, GET, Centre National de la Recherche Scientifique, Institut de Recherche pour le Développement, Université Toulouse III Paul Sabatier, Université de Toulouse, Toulouse, France, [2]ISTerre, Centre National de la Recherche Scientifique, Université Grenoble Alpes, Grenoble, France, [3]Department of Earth Sciences, University of Oregon, Eugene, OR, United States, [4]Faculty of Earth Sciences, University of Iceland, Reykjavik, Iceland, [5]Scientific and Technological Centers, Universitat de Barcelona, Barcelona, Spain, [6]UAR Raimond Castaing, Centre National de la Recherche Scientifique, Institut National Polytechnique de Toulouse, Université Toulouse III Paul Sabatier, Institut National des Sciences Appliquées de Toulouse, Université de Toulouse, Toulouse, France

Active felsic magmatism has been rarely probed *in situ* by drilling but one recent exception is quenched rhyolite sampled during the 2009 Iceland Deep Drilling Project (IDDP). We report finding of rare zircons of up to ~100 μm in size in rhyolite glasses from the IDDP-1 well products and the host 1724 AD Viti granophyres. The applied SHRIMP U-Th dating for both the IDDP and the Viti granophyre zircons gives zero-age (±2 kyr), and therefore suggests that the IDDP-1 zircons have crystallized from an active magma intrusion rather than due to the 20–80 ka post-caldera magmatic episodes recorded by nearby domes and ridges. Ti-in-zircon geothermometer for Viti granophyre reveals zircon crystallization temperatures ~800°C–900°C, whereas IDDP-1 rhyolite zircon cores show Ti content higher than 100 ppm, corresponding to temperatures up to ~1,100°C according to the Ti-in-zircon thermometer. According to our thermochemical model at such elevated temperatures as 1,100°C, rhyolitic magma cannot be saturated with zircon and zircon crystallization is not possible. We explain this controversy by either kinetic effects or non-ideal Ti incorporation into growing zircons at low pressures that start to grow from nucleus at temperatures ~930°C. High temperatures recorded by IDDP-1 zircon together with an occurrence of baddeleyite require that the rhyolite magma formed by partial melting of the host granophyre due to basaltic magma intrusion. Zr concentration profiles in glass around zircons are flat, suggesting residence in rhyolitic melt for >4 years. In our thermochemical modeling, three scenarios are considered. The host felsite rocks are intruded by: 1) a basaltic sill, 2) rhyolite magma 3) rhyolite sill connected to a deeper magmatic system. Based on the solution of the heat conduction equation accounting for the release of latent heat and effective thermal conductivity, these data confirm that the rhyolite magma could be produced by felsic crust melting as a result of injection of a basaltic or rhyolite sill during the Krafla Fires eruption (1975 AD).

KEYWORDS

Iceland Deep Drilling Project, IDDP-1 sample, zircon, rhyolite magma genesis, U-Th age, granophyre, melting, thermochemical modeling

Introduction

Icelandic volcanic activity represents an excellent example of a basalt-dominated environment where felsic crust can be produced either due to progressive cooling and interaction with rocks affected by both hydrothermal fluids and basaltic magmatism (e.g., Torsvik et al., 2015; Foulger et al., 2020) or by rejuvenation of the pre-existing continental crust by partial melting (Foulger et al., 2020). The low-$\delta^{18}O$ character of Icelandic felsic magmas suggests generation by open-system processes of partial melting of the hydrothermally-altered basaltic crust and melt-fluid-rock interactions (Jónasson, 1994; Gunnarsson et al., 1998; Bindeman et al., 2012; Pope et al., 2013). Other petrogenetic processes involved in the formation of felsic magmas include crustal assimilation coupled with fractional crystallization, and near-solidus differentiation (Nicholson et al., 1991; Jónasson, 2007; Elders et al., 2011; Pope et al., 2013; Hampton et al., 2021). Furthermore, magma mixing and the following hybridization have been documented and acted as a potential trigger for volcanic eruptions (e.g., Borisova et al., 2012 and references therein). Recently, Rooyakkers et al. (2021; 2022) evoked that a plate boundary rifting events and the related mafic recharges trigger hybrid to felsic eruptions of Krafla.

Natural data and experiments on crystallization of Icelandic glassy rhyolite and finely-crystallized (≤1 mm) granophyre partial melting demonstrate efficient partial melting of the felsic crust (e.g., Masotta et al., 2018), and efficient assimilation of hydrothermally altered crust (Hampton et al., 2021). Masotta et al. (2018) suggest that the IDDP-1 (Figure 1) rhyolite magma could originate from a high-degree partial melting of felsic rocks rich in quartz and feldspars by a basaltic intrusive event. Alternatively, the numerical model of Simakin and Bindeman (2022) based on $\delta^{18}O$ and δD allows two possible scenarios for IDDP-1 rhyolite production through interaction with *i*) overheated rhyolite or *ii*) basaltic magma. Subsequently, the IDDP-1 rhyolitic magma may have been

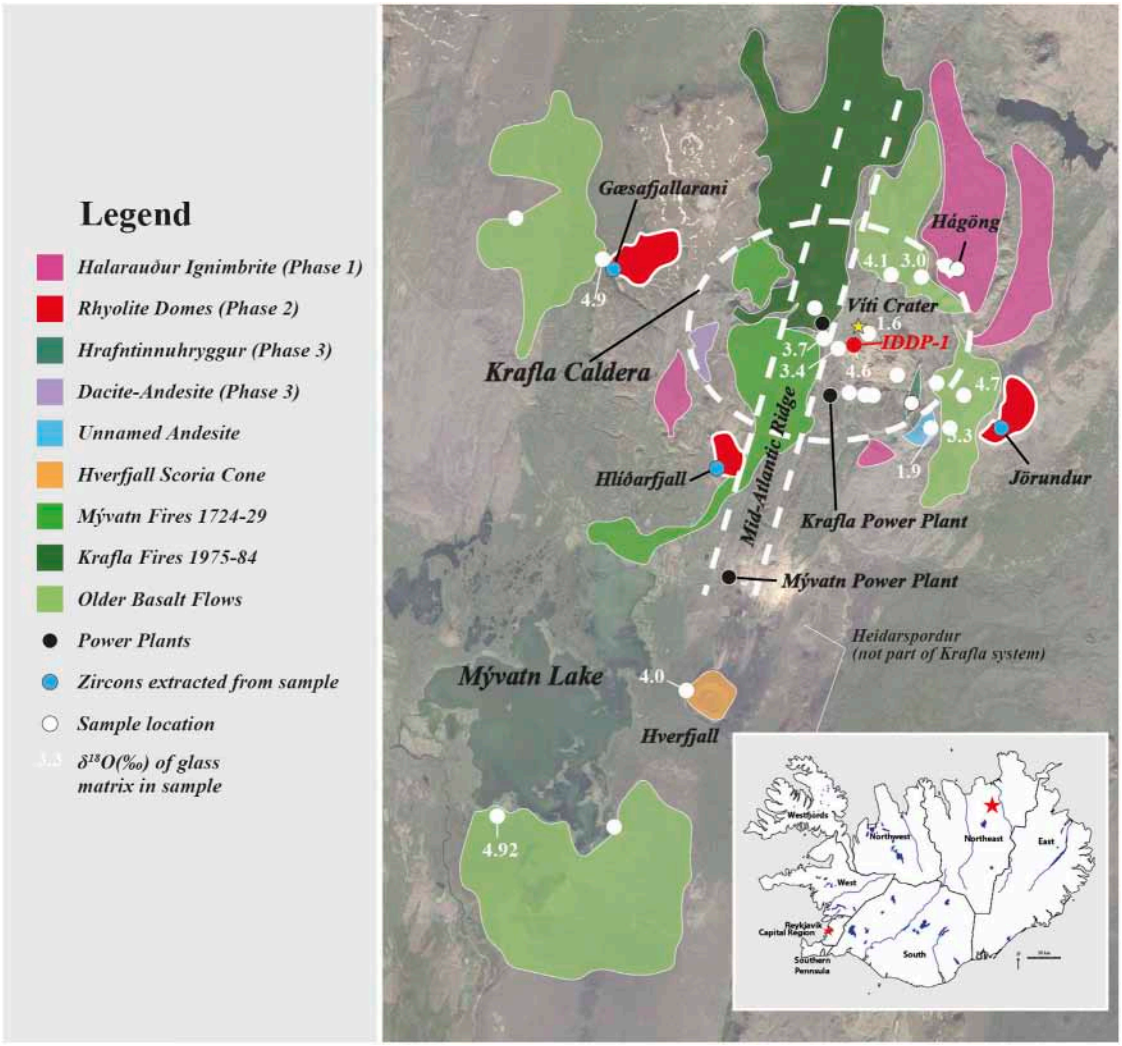

FIGURE 1
Geological map showing the Krafla caldera that is located in the Northeastern Iceland (see insert map) (modified after Hampton et al., 2021). The location of the IDDP-1 well and the Viti Crater are shown (see Supplementary Material).

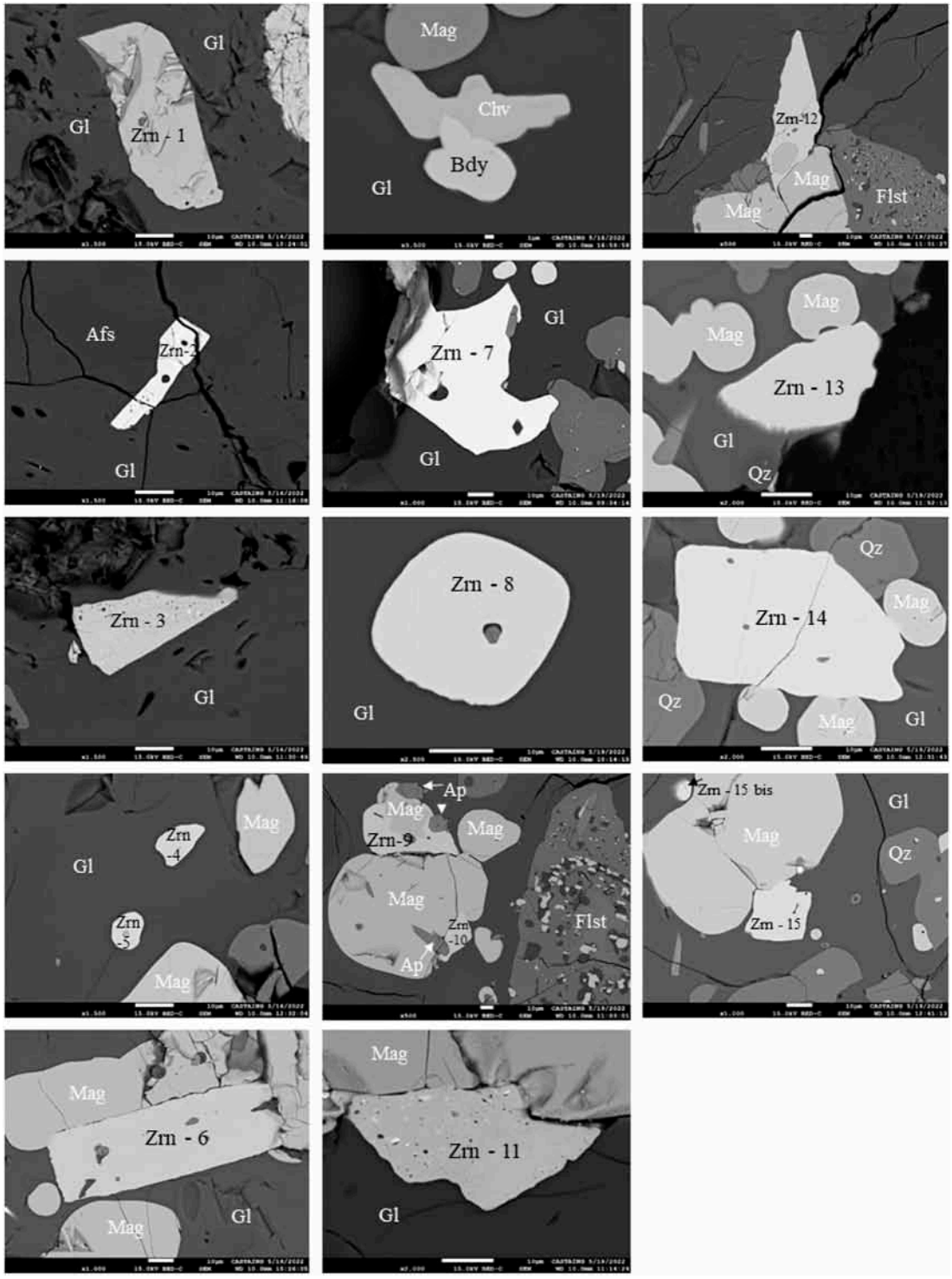

FIGURE 2
Representative backscattered electron (BSE) images of the IDDP-1 zircon (Zrn) and baddeleyite (Bdy) crystals discovered during the SEM sessions (FEG JEOL JSM 7100F TTLS LV SEM at the Center Castaing, Toulouse, France). Zrn, zircon; Bdy, baddeleyite; Chv, chevkinite; Flst, partially melted and residual felsite; Gl, silicate glass of rhyolitic composition; Mag, titanomagnetite; Ap, apatite; Afs, alkali feldspar; Qz, quartz. The scale bars correspond to 10 μm (except for the BSE image with baddeleyite, Bdy, where the scale bar is of 1 μm).

formed at shallow crustal level due to partial melting of the crystalline host rocks. However, no zircon study on the IDDP-1 nor Viti granophyre samples has been performed and the existing data and models do not capture the mechanisms of thermochemical exchange due to the basaltic intrusion(s) nor when the currently molten rhyolite magma was produced.

We report here for the first time the results from an investigation of rare zircon crystals in the IDDP-1 rhyolite sample. We compared these

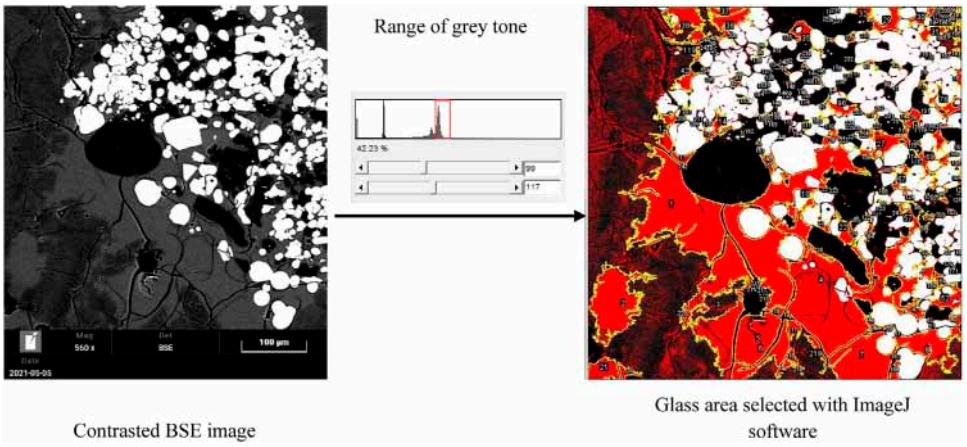

FIGURE 3
Example of glass (quenched silicate melt) fraction calculation. In each zircon-bearing zone, the glass fraction is calculated using BSE images of low magnification.

zircons with those in the host Viti granophyre through micro-analytical and modeling approaches to better constrain the timescales and mechanisms of rhyolite magma production at Krafla volcano. The obtained data point to very recent zircon crystallization, implying that these grains were resident in an active magma reservoir and potentially among the youngest zircons ever studied in the currently active rift volcanic system, likely comparable to those of the mid-ocean ridges (e.g., Bea et al., 2020). Our analytical results coupled to geochemical and thermochemical modelling shed new light on the origin of Icelandic rhyolites and the timescales of zircon formation in silicic melts.

Materials and methods

During the Iceland Deep Drilling Project well 1 (IDDP-1) drilling near the Viti Crater (Figure 1), beyond ~2,100 m depth the dominant fragments were dark brown glass shards interpreted to have quenched by melt interaction with the drilling water. Analysis of these cuttings indicated that the rhyolite melt was emplaced into crystalline felsic intrusive rocks called felsite or granophyre (e.g., Zierenberg et al., 2013). The IDDP-1 rhyolite sample and five host Viti granophyre samples were investigated. The IDDP-1 sample consists of the predominant brown rhyolite glass with plagioclase, two pyroxenes, titanomagnetite, ilmenite and/or apatite forming glomerocrysts and rare zircon grains (Figure 2); quartz and alkali feldspar show textural evidence for resorption, and were previously interpreted by Zierenberg et al. (2013) as xenocrysts. The analytical, imaging and Th-U dating data, and modeling parameters and data are summarized in Supplementary Material and Supplementary Tables S1–S8 and displayed in Figures 3–8. Average compositions of the rhyolite glass and of one representative Viti granophyre sample are given in Table 1.

Zircon and baddeleyite crystals

Most of the studied zircons are small (20–60 μm in size, reaching a maximum of 100 μm) and have euhedral, subhedral to anhedral morphologies (Figures 2, 4A, B). The morphology and the internal oscillatory zoning suggest that the crystals are of magmatic origin. Electron probe microanalysis, EPMA spot analyses and mapping show that the zircon crystals are variably enriched in Fe, Al, P, Hf, Y. Two larger crystals (Z1 and Z3) have inclusions of Si-Al-rich glasses (72–83 wt% SiO_2; 5–11 wt% Al_2O_3), britholite (Ce, Ca, Th, La, Nd)$_5$(SiO_4, PO_4)$_3$(OH,F) and chevkinite ((Ce, La, Ca, Th)$_4$(Fe^{2+}, Mg)$_2$(Fe^{3+})$_3$$Si_4O_{22}$) phases, which are rich in P, Al, Fe and Y. The analyzed Ti concentrations in the zircon crystals, far from the visible inclusions, range from ~35 ppm (in rims) to 230 ppm (in cores) (n = 35, n being the number of analyses) with an average value of ~125 ppm, which is higher than those previously observed in Icelandic zircons (up to 60 ppm, e.g., Carley et al., 2022) and corresponds to much higher crystallization temperatures (up to 1,000°C–1,100°C) for the rhyolite magma. For example, the application of the Ti-in-zircon geothermometer of Ferry and Watson (2007) assuming activities of a_{SiO2} = a $_{TiO2}$ = 1 and 106 ppm gives minimal estimates of ~1,030°C (Figure 4A). Among similar zircon crystals, we filtered those hosted by pure rhyolitic glass and without any trace of Fe-Ti-bearing minerals and glass inclusions (Figure 4A). The IDDP-1 zircons yield "zero" aged ^{238}U-^{230}Th dates for crystallization, with an uncertainty of ±2,000 years (Figure 4B; Supplementary Table S7). Zircon sizes and glass fractions (Figures 3, 5) were investigated to constrain the mechanism of the rhyolite formation based on the thermochemical modelling of zircon behavior presented below. The compositional features of the IDDP-1 zircons were also compared to those of the host Viti granophyre (Ti contents range from ~23 ppm in rims up to 43 ppm in cores), which corresponds to much lower crystallization temperatures (800°C–900°C) for the host granophyre magma. Most of the Viti granophyre zircons yield zero-age isochron dates such as the IDDP-1 sample, but several crystals yield older model dates of ~8–13 ka and up to ~150 ka (Supplementary Table S7; Figure 4B).

The measured Zr contents in the glasses surrounding several analyzed zircon crystals from the glass-zircon interface up to 60–100 μm into the glass show flat concentration profiles and if any, very weak gradients (Figure 6). The data were corrected for secondary fluorescence using the program FANAL (Llovet et al., 2012; Borisova et al., 2018). Zr concentrations in the glass around

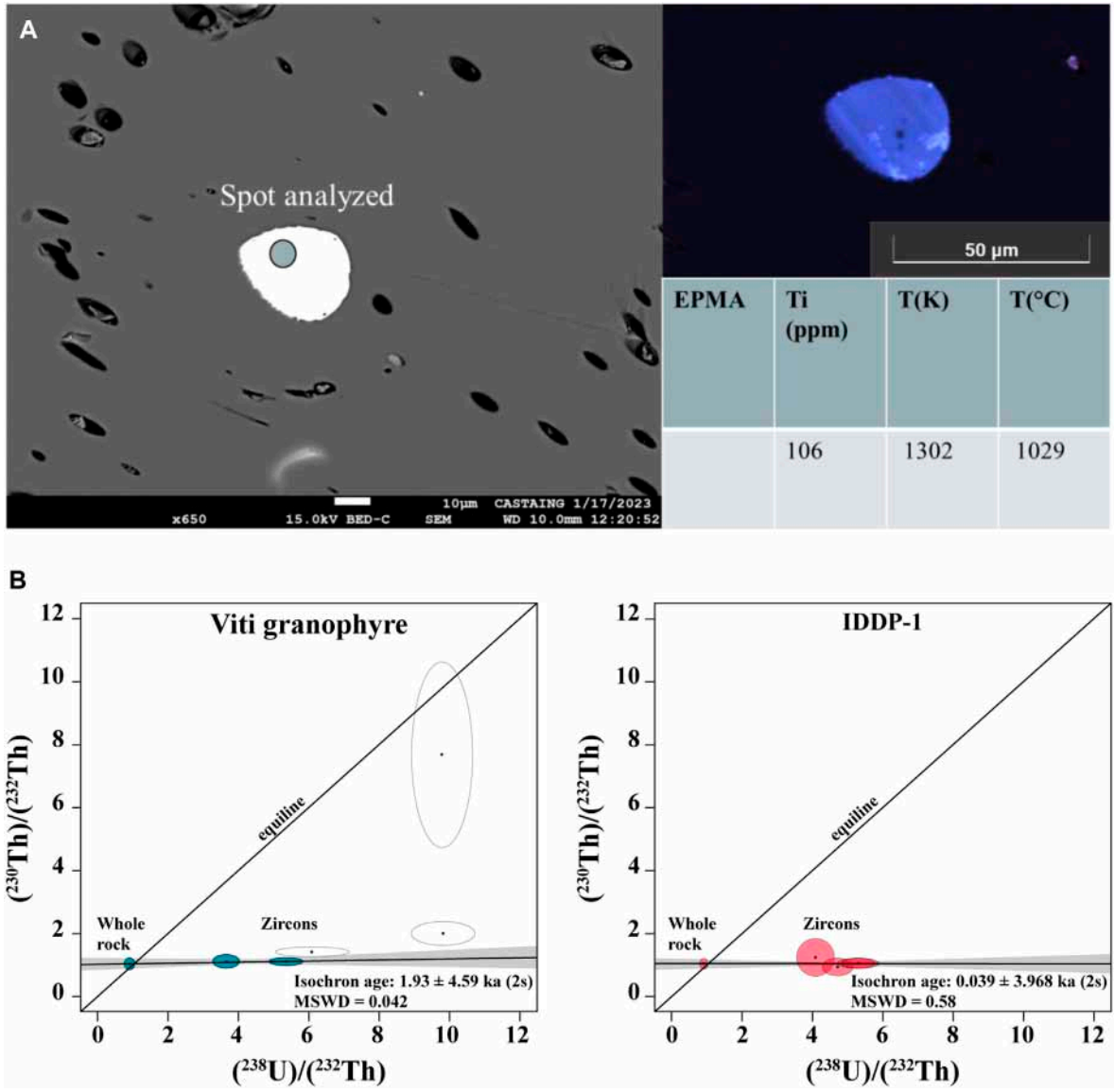

FIGURE 4
(A) Backscattered electron and cathodoluminescence images of a representative IDDP-1 zircon (Zrn-83 of series 4) surrounded by rhyolite glass. Zrn, zircon. Ti contents in the IDDP-1 zircons and temperature estimates calculated according to the Ti-in-zircon thermometer (Ferry and Watson, 2007) are shown. **(B)** U-Th isochron diagrams for *in-situ* analyses of zircons from Viti granophyre and IDDP-1 rhyolite sample (discovered during the first and the second SEM session). Isochron dates are derived using shaded data for whole rocks and individual zircons with dates calculated using IsoplotR (Vermeesch, 2018). Each datum represents an *in-situ* analysis of a single zircon crystal. Error ellipses are 2σ.

different zircons overlap, suggesting no significant differences in the patterns within this IDDP-1 sample. Overall, the Zr concentration level in the glass is ~420 ppm according to EPMA and 400 ± 50 ppm according to femtosecond laser ablation inductively coupled plasma (fs LA-ICP-MS) (Table 1), which corresponds to zircon saturation temperatures of 830°C–870°C depending on the solubility model used (e.g., Watson and Harrison, 2005) (Supplementary Table S5). This discrepancy between this estimate of crystallization temperatures and the much higher Ti-in-zircon temperatures (>1,000°C, see above) will be discussed below. Observation of several baddeleyite (xeno)crystals in the IDDP-1 glass sample (Figure 2) implies an involvement of mafic (e.g., basaltic) magma rather than hot rhyolite in the magmatic system.

Thermochemical and geochemical modeling of zircon behavior

In order to confirm the plausible scenario of the formation of Krafla rhyolite, a thermochemical model of heat transfer from a convecting magmatic intrusion to felsic (granophyric) host rocks involving melting and production of the hot rhyolite magma was developed. The model is based on the solution of a the 1D heat conduction general equation with account for the release of the latent heat of crystallization and convection in a two layered system of contrasting (in the case of the injection of a basaltic magma) compositions. The lower layer contains initially injected magma that releases heat to the surrounding felsic rocks. The model uses phase

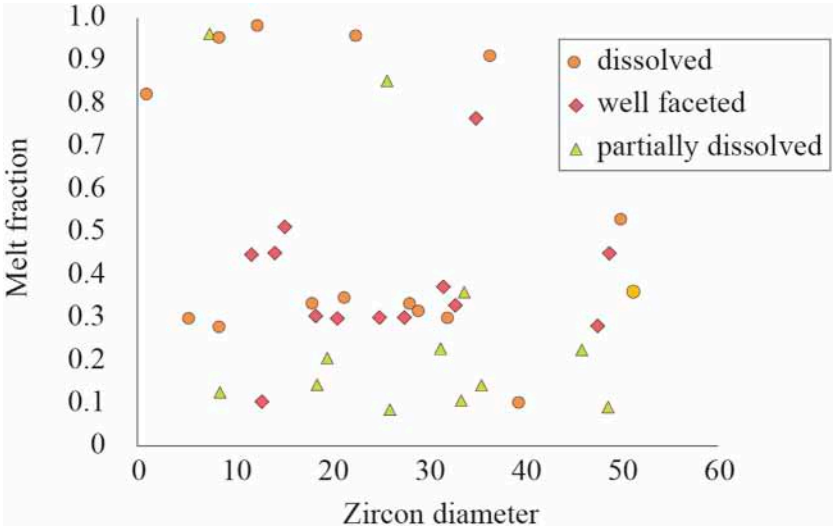

FIGURE 5
Silicate glass (quenched melt) fraction versus zircon diameter (in μm) calculated for the IDDP-1 rhyolite sample. Three types of the zircon were distinguished according to the morphology: 1) dissolved, 2) well faceted and 3) partially dissolved zircon crystals.

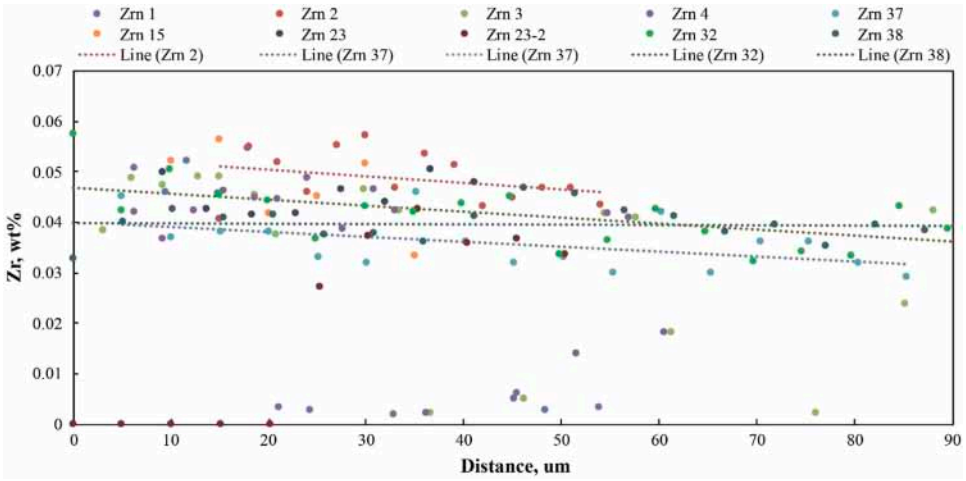

FIGURE 6
Zr concentration profiles (in wt%) along lines across the glass adjacent to the IDDP-1 zircons, corrected for the effect of secondary fluorescence, suggesting at least 4 years of the zircon-bearing rhyolite magma storage. Distance (in μm) corresponds to the distance from the zircon-glass interface.

diagrams for Krafla basalt and the Viti granophyre (melt fraction versus temperature) produced using of the Rhyolite-MELTS software (Gualda et al., 2012, https://melts.ofm-research.org/).

The system of equations has the following form:

$$\rho_i C_i \frac{\partial T}{\partial t} = \frac{\partial}{\partial x} k_i \frac{\partial T}{\partial x};\ C_i = C_i^0 + \frac{\partial X_i}{\partial T} L\star^i;$$

$$k_i = k_i(Nu_i, T);\ Nu_i = \frac{Q_{conv}}{Q_{cond}} = \omega * Ra_i^{1/3};$$

$$Ra = \frac{\rho\beta\Delta T h^3}{\kappa\mu(T,X)};\ \kappa = \frac{k_m}{\rho C_i}$$

Here ρ is the density of magma, C is the heat capacity, T is the temperature, X is the crystal content, L^* is the latent heat of crystallization, k is the thermal conductivity, Nu is the Nusselt number, Ra is the Rayleigh number, ω ~0.1–0.3 is a proportionality constant, index i =1,2 corresponds to basaltic and rhyolitic layers, respectively, x is distance and t is time. The Rayleigh number for basalt is calculated based on the thickness h equal to the half width of the injected sill; h for the rhyolitic layer is calculated based on the thickness of the molten felsic crust (melt fraction greater than 95%). The temperature difference between the center of the basaltic sill and the basalt-rhyolite interface is taken as characteristic for ΔT for i = 1, we calculate the mean temperature in the rhyolitic layer $<T_r>$ and assume that $\Delta T = <T_r> - T_{rm}$, where T_{rm} is the temperature that corresponds to 5% melting of the felsite. The effective thermal conductivities are parametrized based on Turner's correlation (Turner, 1979). They

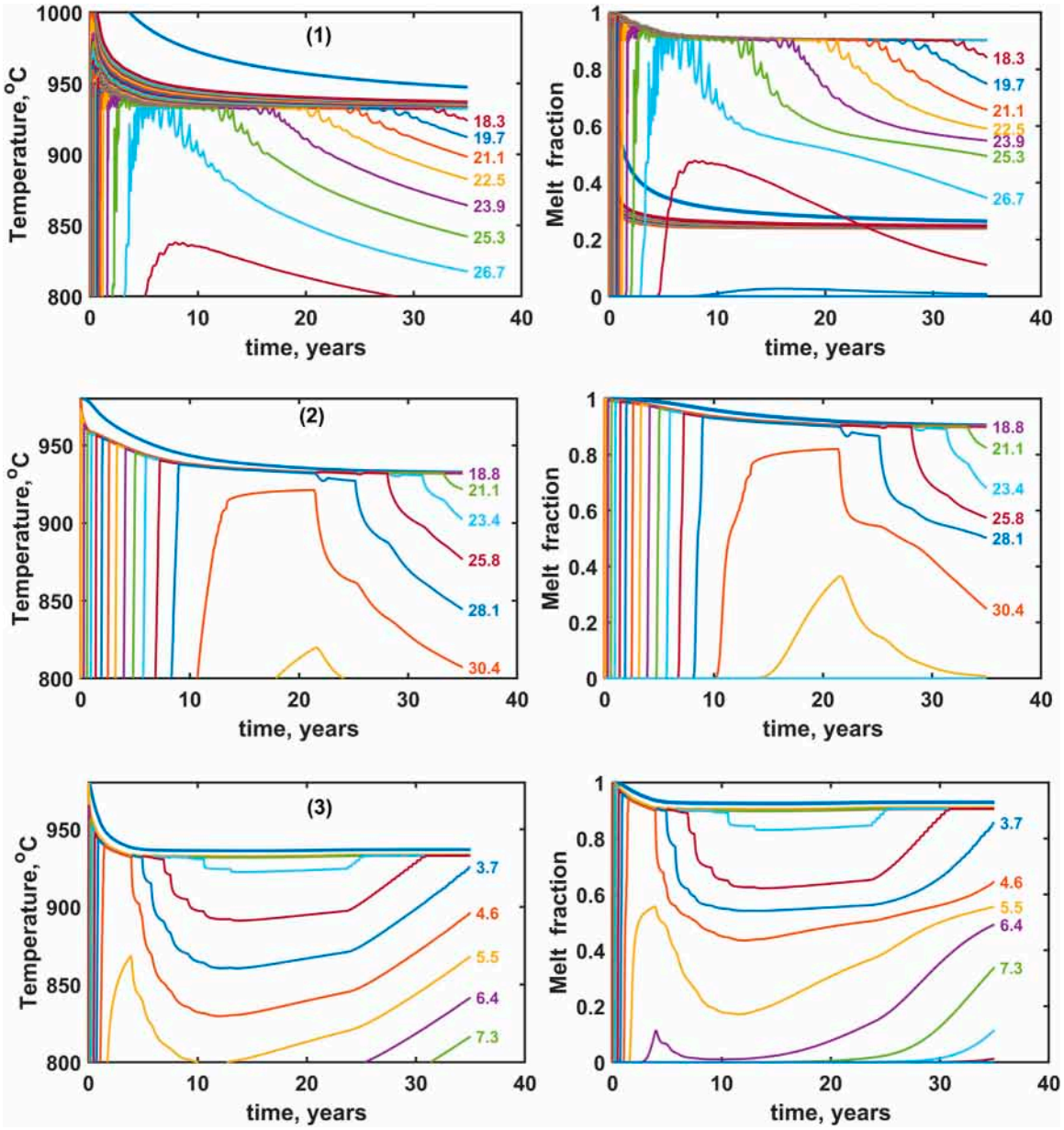

FIGURE 7
Temperature (in °C) and melt fraction versus time (in years) for three scenarios: 1) injection of the basaltic sill of a thickness of a 100 m at initial temperature of 1,150°C. 2) injection of a 900 m rhyolitic sill with the initial temperature of 980°C; 3) the same as (2) but the thickness of the sill is 100 m and the heat flux at the bottom of 12 W/m^2. Thick lines correspond to the basaltic magma for scenario (1), for the center of the sill for scenario (2) and for the bottom of the sill for scenario (3). Thin lines are labeled as a distance (in m) from the contact between the injected magma and host rocks.

are up to 3 orders of magnitude larger than the thermal conductivities resulting in efficient temperature homogenization in the convective layers. In the case of rhyolitic magma injection convection occurs in a single layer. The temperature difference between the center of the sill and T_{rm} is used as a characteristic temperature. Viscosities of basaltic and rhyolitic magmas are calculated using the model from Giordano et al. (2008) with a correction to account for the crystal content by Costa et al. (2009).

Simulation parameters are summarized in Supplementary Table S8. We assume symmetry boundary condition at the center of the injected sill and a constant far field temperature in felsite. The outer boundary was chosen far enough to avoid any influence on the temperature distribution in molten layers. Also, the case of a rhyolitic sill connected to a deep magmatic system is considered. In this case, a constant heat flux at the bottom of the sill is specified.

Based on the temperature histories produced by the thermochemical modeling, zircon dissolution and growth simulations were also carried out following the methods of Bindeman and Melnik (2016; 2022). The model accounts for the experimentally determined equilibrium saturation of silicate melt with zircon and the Zr diffusion coefficient in the silicate melts. The

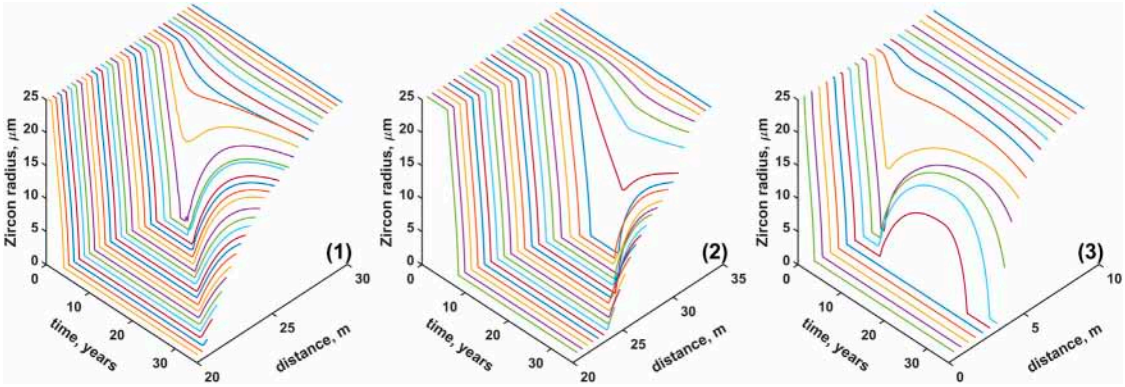

FIGURE 8
Dependence of the zircon radius on both time and distance from the initial contact between the injected magma and host rocks, for the three different scenarios considered (see Figure 7 for full description). At small distances between the contact, zircons dissolve completely, at larger distances they start to regrow, and far away only a limited dissolution of the crystals occurs. For scenario (3) at later stages of the system, evolution growth at intermediate distances switches to dissolution due to progressive heat flux from the deep feeding system.

1D transient diffusion equation is solved inside the melt shell surrounding the growing zircon. The MatLab code is available from https://github.com/crystalworkshop/krafla_sill.

For the geochemical modelling (Supplementary Table S3) of residence times from the Zr profiles surrounding the IDDP-1 zircon crystals, we have applied the diffusion equation $t \sim X^2/D$ (e.g., Crank, 1979), where t is the duration (s), X is the distance (μm) and D is the Zr diffusion coefficient in m^2/s. Residence times calculated with Zr diffusion according to Zhang and Xu (2016) at 900°C gives maximal values of 4 years, suggesting stable conditions of neither growth nor dissolution of zircon prior to sampling by the IDDP-1 borehole in 2009.

Implications for the IDDP-1 rhyolite formation

The maximal duration of rhyolite magma storage may correspond to a period from the beginning of last intrusion of basaltic magma (Krafla Fires, 1975 basaltic intrusions and lavas), which corresponds to 34 years before the IDDP-1 sampling in 2009. The melt batch that was sampled by IDDP-1 glass was likely in thermal contact for up to 34 years with the intruded sill. The uncertainty on the IDDP-1 rhyolite age (±2.0 kyr) does not allow us to distinguish between the Krafla Fires and the phreatomagmatic event during the opening phase of the Mývatn Fires, forming the crater Víti in 1724. In this work, we tested a hypothesis and performed thermochemical modeling of a basaltic or rhyolite intrusion interaction with the host granophyre rock directly related to the 1975 Krafla Fires event. The combined scanning electron microscopy (SEM)-EPMA-LA-ICP-MS-SHRIMP data provide evidence for the formation of the IDDP-1 rhyolite through high-temperature melting of granophyre rock by near-zero-age intrusion of a hot basaltic magma.

The results from thermochemical simulations presented below predict that the heat released from the intruded magma is sufficient for melting of felsite and formation of rhyolitic melt. After a critical melt layer thickness is reached, it begins to convect. Three scenarios are considered. The host felsite rocks are intruded by: 1) a basaltic sill, 2) rhyolitic magma 3) rhyolitic sill connected to a deeper magmatic system. In all scenarios the emplacement occurs during 1975–1983 Krafla Fires eruption and the system evolves for 35 years. The measured temperature distribution (Eichelberger, 2019) in the vicinity of the intrusion is used for model calibration. Sharp temperature gradient near the contact with magma requires intense convection in the magma body for at least 35 years. We use this constraint to estimate the necessary thickness of the intruded sill.

Scenario (1). The density of the rhyolitic melt remains smaller than the density of the basalt and prevents intense mixing between the two magmas by Rayleigh-Taylor instability. An example of the temperature and melt fraction evolution with time is shown in Figure 7, top panels for a system with the starting basaltic layer of 100 m thick at 1,150°C. We assume that the basalt is intruded at liquidus conditions at ~ 1,150°C. We also suggest a thickness of 100 m to fit the temperature profile recorded in the Krafla region (Eichelberger, 2019). Numbers on Figure 7 represent the distance from the initial interface between the magma and the wall rocks. Basaltic magma triggers the melting of ~27 m-thick felsic rocks in a matter of 5 years. The basaltic layer crystallizes significantly (Figure 7, top panel) after ~7 years of cooling and the convection in this layer slows down the rate of heat transfer to the rhyolite convecting above. The melting of the felsite rock slows down, and the upper layer starts to solidify. Basaltic magma cools and crystallizes quickly, while the temperature in the upper felsic layer evolves more slowly. Convection proceeds during the whole simulated period, although the width of the layer and the intensity of the convection decrease. After 35 years, the melt fraction in basaltic magma decreases to less than 0.3, while the crystallinity (inverse function of the melt fraction) of the felsic magma layer remains lower (0.1–0.6, depending on the distance from the contact with basaltic sill). The melt fractions of the rhyolite magma reproduce the real glass fractions estimated in the rhyolite glass of the IDDP-1 sample (Figure 5).

TABLE 1 Composition of the 2009 IDDP-1 glasses and the associated Viti granophyre.

Sample number	IC-82**	IDDP-1***	IDDP-1****	1σ uncertainty
	Viti granophyre	Rhyolite glass (Gl)	Rhyolite glass (Gl)	Rhyolite glass (Gl)
	bulk-rock	EPMA*	fs LA-ICP-MS*	fs LA-ICP-MS
		(265 points)	(145 points)	(145 points)
SiO_2 wt%	74.71	74.65 ± 0.67	68.25 ± 1.55	8.68
TiO_2	0.47	0.33 ± 0.02	0.35 ± 0.01	0.04
Al_2O_3	11.95	11.31 ± 0.15	11.30 ± 0.00****	—
FeO	N.A.	2.91 ± 0.11	3.01 ± 0.09	0.39
Fe_2O_3	3.66	N.A.	N.A.	N.A.
MnO	0.08	0.07 ± 0.03	0.064 ± 0.002	0.01
MgO	0.35	0.21 ± 0.03	0.20 ± 0.01	0.025
CaO	1.84	1.47 ± 0.06	1.43 ± 0.04	0.19
Na_2O	4.06	3.86 ± 0.16	3.54 ± 0.08	0.45
K_2O	2.65	2.88 ± 0.08	3.48 ± 0.36	0.45
P_2O_5	D.L.	0.05 ± 0.03	0.038 ± 0.004	0.006
Total	99.77	97.75 ± 0.78	N.A.	N.A.
Ba ppm	476	N.A.	494.87 ± 8.74	62.10
Ce	80.6	N.A.	80.62 ± 2.12	10.00
La	39.6	N.A.	38.60 ± 0.96	4.67
Nb	29.1	N.A.	34.94 ± 6.43	4.13
Nd	38.5	N.A.	37.57 ± 1.18	4.64
Rb	64.4	N.A.	73.32 ± 2.49	9.55
Sr	72.9	N.A.	58.65 ± 1.59	7.25
Y	61.1	N.A.	62.33 ± 1.28	7.59
Zn	74.3	N.A.	N.A.	N.A.
Zr	425	N.A.	407.52 ± 8.68	50.23
U	1.99	N.A.	2.17 ± 0.11	0.29
Th	6.72	N.A.	7.38 ± 0.20	0.93
H_2O bulk	0.13	1.9[$]	N.A.	N.A.
CO_2 bulk	0.08	N.A.	N.A.	N.A.
S bulk	<0.01	N.A.	N.A.	N.A.

*Electron probe microanalysis (EPMA) and femtosecond laser ablation inductively coupled plasma (fs LA-ICP-MS) analysis data.
**N.A., not analyzed; D.L., value below detection limit.
***EPMA, data obtained in this work.
****fs LA-ICP-MS, data. Al_2O_3 was used as the internal standard for the major and trace element quantification by SILLS, standard deviation correspond to the sample heterogeneity, which is smaller than the analytical uncertainty.
[$]Data from Pope et al. (2013).

Scenario (2). In order to keep intensive convection during 35 years of the evolution, the required system has to be composed of the rhyolitic layer with thickness exceeding of 900 m at the temperature of 980°C, which definitely conflicts with geophysical observations (Kim et al., 2020). A thinner layer, which significantly solidifies at the top and the temperature gradient in the host rocks, will become much smoother than that observed during drilling. The thickness of the molten felsic crust in this scenario exceeds 30 m after 21 years and decreases to 18 m at the end of the simulation period (Figure 7, middle panels).

Scenario (3). An alternative to the thick rhyolitic layer, a thin (100 m) layer of rhyolitic magma with a heat supply from a deeper magmatic system can be considered (Figure 7, bottom panels). To retain high convection intensity, the necessary heat flux is estimated to be 12 W/m^2. A magma intrusion rate that supports such heat flux

would require an uplift of 9 cm/year over observation period. The rhyolite sill stays close to a steady state with only 4 m of the molten crust produced over 35 years. The temperature of the magma after 20 years of cooling starts to increase slowly due to permanent heat influx. The temperature difference between the bottom and the top of the injected rhyolite magma remains within 5°C due to intense mixing.

Based on the calculated temperatures, we simulate diffusive growth of zircon crystals in molten felsic crust. Because the model does not simulate convection directly, we cannot obtain temperature histories in the individual batch of rhyolite magma, but only at fixed distances from the initial contact between the magma and host rocks. Intensive convection will result in migration of magma batch within the layers and, thus, more complicated thermal evolutions. Although calculated temperatures can be treated only as end-member cases, they shade light on zircon dissolution/growth during felsic crust melting.

Depending on the distance from the contact between the injected magma and the molten felsite, zircons experience different degrees of melting and consequent growth (Figure 8). For scenario (1) at distances less than 23 m, zircon crystals dissolve completely after a few years and do not regrow during 35 years. At larger distances different proportions of zircon cores are preserved. Regrowth of zircons occurs when magma becomes supersaturated with zircon at temperatures of ~900°C–950°C, depending on zirconium bulk content and solubility model. The final size of the crystals depends on the distance from the contact ranging from a few microns to a nearly complete recovery after heat shock, but the zircon age record can be partly removed during dissolution. At distances larger than 27 m, only dissolution of zircons takes place at later stages of the system evolution.

Scenario (2) shows a similar behavior to that of scenario (1) at slightly bigger distances from the initial contact between the magma and the rock. However, in the case of rhyolitic magma injection, convective mixing will occur inside the whole 900 m-thick sill and the zircon crystals will not be preserved. In scenario (3), progressive heating of the system by the influx of hot magma from below results in zircon dissolution in the whole simulated domain.

The timescale required to generate the profiles recorded in the IDDP-1 rhyolite glasses around the idiomorphic crystals of zircon was estimated (Figure 6). Modeling of the residence timescale to flatten Zr profiles generated upon the zircon crystallization/dissolution suggests that any time of >4 years and definitely of <34 years, is sufficient to generate the observed Zr profiles by re-equilibration of the rhyolite melts once the zircon-melt system achieves a stable configuration (Supplementary Table S3). This timescale is in an agreement with the prediction of the thermochemical model.

Zircon crystals that regrow after a complete dissolution in all three scenarios experience extremely fast growth rates at small radii (Figure 8). At later stages, the growth rate decreases significantly and the concentration profiles around zircons become smoother. The drastic increase in Ti contents in the cores of completely resorbed and regrown zircons can be explained either by non-equilibrium Ti partitioning between zircon and melt at highly elevated growth rates or by crystallization of major minerals that enrich the surrounding melt with zirconium and other incompatible elements (Bea et al., 2022). The second option conflicts with the phase diagram for Krafla rhyolite, because these temperatures are well above the liquidus. Basaltic magma should have extremely high Zr contents to become supersaturated with zircon at only 10% reduction of the melt fraction (e.g., Borisova et al., 2020).

The first option requires more theoretical and experimental studies. The dependence of the partition coefficient on the growth rate is well known in different magmatic systems. Phosphorus enrichment in olivine crystals can be explained by this mechanism (Shea et al., 2019). Mollo et al. (2011) experimentally observed non-equilibrium trace element partitioning in plagioclase-melt systems. There are no studies on the non-equilibrium partition of Ti in zircons because large typical felsic magmatic systems do not experience such rapid zircon growth as occurred on Krafla volcano. Additionally, a non-equilibrium or non-Henry's law behavior of Ti-in-zircon together with preferred incorporation of Ti at very low pressures corresponding to the crustal levels (Fu et al., 2008) can explain the elevated Ti contents in zircon cores. Alternatively, nano inclusions of Ti-rich phases such as magnetite or rutile during fast growth can be incorporated into growing crystals. As we examined zircons under the SEM only down to 50 nm resolution, these nano-inclusions could significantly contribute to the apparent Ti concentrations measured by EPMA.

The presence of a baddeleyite (xeno)crystal in the IDDP-1 rhyolite (Figure 2) implies its formation within mafic (low activity of SiO_2, $a_{SiO2} < 1$) rather than felsic (high $a_{SiO2} = 1$) magma. In this case, the baddeleyite crystal can be also interpreted as a proxy of hydrothermal alteration of Zr-bearing phases in the host felsite. However, no baddeleyite crystal was found in the host Viti granophyre and thus this mineral could be a proxy of a mafic source. The 1975 AD eruptions record massive basaltic intrusions, implying that the occurrence of the IDDP-1 baddeleyite crystal is generated by the basalt-granophyre rock interaction. The proposed thermochemical model demonstrated in Figure 7 involves melting of the host granophyre by the hot magma intrusion. The IDDP-1 rhyolite melts produced cool and undergo equilibrium crystallization of silicates and oxides. Our model thus explains how the rhyolite magma can be produced in the hybrid Icelandic crust due to the present-day magmatic activity.

Data availability statement

The original contributions presented in the study are included in the article/Supplementary Material, further inquiries can be directed to the corresponding author.

Author contributions

AYB: Conceptualization, Funding acquisition, Investigation, Methodology, Project administration, Supervision, Validation, Writing–original draft, Writing–review and editing. OEM: Methodology, Software, Writing–review and editing. NG: Investigation, Formal Analysis, Methodology, Writing–review and editing. INB: Funding acquisition, Investigation, Methodology,

Writing–review and editing. TT: Investigation, Methodology, Formal Analysis, Writing–review and editing. MR: Investigation, Methodology, Formal Analysis, Writing–review and editing. AS: Funding acquisition, Resources, Writing–review and editing. OL: Investigation, Methodology, Writing–review and editing. ML: Formal Analysis, Investigation, Methodology, Writing–review and editing. XL: Investigation, Methodology, Writing–review and editing. PP: Writing–review and editing. AP: Investigation, Methodology, Writing–review and editing. ST: Methodology, Supervision, Writing–review and editing.

Funding

The author(s) declare financial support was received for the research, authorship, and/or publication of this article. This work was supported by the Institut Carnot ISIFoR (TRACENEO project), and the INSU-CNES project PLAGIOGRAN (2022–2023) to AYB. INB was supported by NSF grant EAR 1822977. XL acknowledges support from grant PID2019-105625RB-C21 funded by MCIN/AEI/10.13039/501100011033. This study has been partially supported through the grant EUR TESS N°ANR-18-EURE-0018 in the framework of the Programme des Investissements d'Avenir. OEM was partially supported by the ERC under the European Union Horizon 2020 Research and Innovation Programme (Grant agreement 787399-SEISMAZE) and College de France PAUSE program (grant #C7H-PUB23A59).

Acknowledgments

Jorge Vazquez (SHRIMP-RG Laboratory, United States) is thanked for U-Th dating. Authors thank A. M. Cousin for the design of all figures.

Conflict of interest

The authors declare that the research was conducted in the absence of any commercial or financial relationships that could be construed as a potential conflict of interest.

Publisher's note

Supplementary material

The Supplementary Material for this article can be found online at: https://www.frontiersin.org/articles/10.3389/feart.2023.1307303/full#supplementary-material

References

Bea, F., Bortnikov, N., Cambeses, A., Chakraborty, S., Molina, J. F., Montero, P., et al. (2022). Zircon crystallization in low-Zr mafic magmas: possible or impossible? *Chem. Geol.* 602, 120898. doi:10.1016/j.chemgeo.2022.120898

Bea, F., Bortnikov, N., Montero, P., Zinger, T., Sharkov, E., Silantyev, S., et al. (2020). Zircon xenocryst evidence for crustal recycling at the Mid-Atlantic Ridge. *Lithos* 354, 105361. doi:10.1016/j.lithos.2019.105361

Bindeman, I. N., Gurenko, A., Carley, T., Miller, C., Martin, E., and Sigmarsson, O. (2012). Silicic magma perogenesis in Iceland by remelting of hydrothermally altered crust based on oxygen isotope diversity and disequilibria between zircon and magma with implications for MORB. *Terra nova.* 24, 227–232. doi:10.1111/j.1365-3121.2012.01058.x

Bindeman, I. N., and Melnik, O. E. (2016). Zircon survival, rebirth and recycling during crustal melting, magma crystallization, and mixing based on numerical modelling. *J. Petrology* 57, 437–460. doi:10.1093/petrology/egw013

Bindeman, I. N., and Melnik, O. E. (2022). The rises and falls of zirconium isotopes during zircon crystallisation. *Geochem. Perspect. Lett.* 24, 17–21. doi:10.7185/geochemlet.2241

Borisova, A. Y., Bindeman, I. N., Toplis, M. J., Zagrtdenov, N. R., Guignard, J., Safonov, O. G., et al. (2020). Zircon survival in shallow asthenosphere and deep lithosphere. *Am. Mineralogist* 105 (11), 1662–1671. doi:10.2138/am-2020-7402

Borisova, A. Y., Freydier, R., Polvé, M., Jochum, K.-P., and Candaudap, F. (2010). Multi-elemental analysis of ATHO-G rhyolitic glass (MPI-DING reference material) by femtosecond and nanosecond LA - ICP - MS: evidence for significant heterogeneity of B, V, Zn, Mo, Sn, Sb, Cs, W, Pt and Pb at mm-scale. *Geostand. Geoanalytical Res.* 34, 245–255. doi:10.1111/j.1751-908X.2010.00077.x

Borisova, A. Y., Toutain, J.-P., Stefansson, A., Gouy, S., and de Parseval, P. (2012). Processes controlling the 2010 Eyjafjallajökull explosive eruption. *J. Geophys. Res.* 117, B05202. doi:10.1029/2012JB009213

Borisova, A. Y., Zagrtdenov, N. R., Toplis, M. J., Donovan, J. J., Llovet, X., Asimov, P. D., et al. (2018). Secondary fluorescence effects in microbeam analysis and their impacts on geospeedometry and geothermometry. *Chem. Geol.* 490, 22–29. doi:10.1016/j.chemgeo.2018.05.010

Burgess, S. D., Coble, M. A., and Vazquez, J. A. (2021). Zircon geochronology and geochemistry of Quaternary rhyolite domes of the Coso volcanic field, Inyo County, California. *J. Volcanol. Geotherm. Res.* 417, 107276. doi:10.1016/j.jvolgeores.2021.107276

Carley, T. L., Bell, E. A., Miller, C. F., Claiborne, L. L., Hunt, A., Kirkpatrick, H. M., et al. (2022). Zircon-modeled melts shed light on the formation of Earth's crust from the Hadean to the Archean. *Geology*. doi:10.1130/G50017.1

Cheng, H., Edwards, R. L., Shen, C. C., Polyak, V. J., Asmerom, Y., Woodhead, J., et al. (2013). Improvements in ^{230}Th dating, ^{230}Th and ^{234}U half-life values, and U–Th isotopic measurements by multi-collector inductively coupled plasma mass spectrometry. *Earth Planet. Sci. Lett.* 371, 82–91. doi:10.1016/j.epsl.2013.04.006

Claiborne, L. L., Miller, C. F., Gualda, G. A. R., Carley, T. L., Covey, A. K., Wooden, J. L., et al. (2018). "Zircon as magma monitor: robust, temperature-dependent partition coefficients from glass and zircon surface and rim measurements from natural systems microstructural geochronology," in *Microstructural geochronology: planetary records down to atom scale: American geophysical union geophysical monograph 232*. Editor D. E. Moser, 3–33. doi:10.1002/9781119227250.ch1

Coble, M. A., Vazquez, J. A., Barth, A. P., Wooden, J., Burns, D., Kylander-Clark, A., et al. (2018). Trace element characterisation of MAD-559 zircon reference material for ion microprobe analysis. *Geostand. Geoanalytical Res.* 42, 481–497. doi:10.1111/ggr.12238

Costa, A., Caricchi, L., and Bagdassarov, N. (2009). A model for the rheology of particle-bearing suspensions and partially molten rocks. *Geochem. Geophys. Geosystems*. doi:10.1029/2008GC002138

Crank, J. (1979). *The mathematics of diffusion*. Oxford University Press.

Eichelberger, J. (2019). Planning an international magma observatory. *Eos* 100, 10–1029. doi:10.1029/2019EO125255

Elders, W. A., Fridleifsson, G. O., Zierenberg, R. A., Pope, E. C., Mortensen, A. K., Gudmudsson, A., et al. (2011). Origin of a rhyolite that intruded a geothermal well while drilling in a basaltic volcano, at Krafla. *Icel. Geol.* 39, 231–234. doi:10.1130/G31393.1

Ferry, J. M., and Watson, E. B. (2007). New thermodynamic models and revised calibrations for the Ti-in-zircon and Zr-in-rutile thermometers. *Contrib. Mineral. Petrol* 154, 429–437. doi:10.1007/s00410-007-0201-0

Foulger, G. R., Doré, T., Emeleus, H., Franke, D., Geoffroy, L., Gernigon, L., et al. (2020). The Iceland microcontinent and a continental Greenland-Iceland-faroe ridge. *Earth-Science Rev.* 206, 102926. doi:10.1016/j.earscirev.2019.102926

Fu, B., Page, F. Z., Cavosie, A. J., Fournelle, J., Kita, N. T., Lackey, J. S., et al. (2008). Ti-in-zircon thermometry: applications and limitations. *Contributions Mineralogy Petrology* 156 (2), 197–215. doi:10.1007/s00410-008-0281-5

Giordano, D., Russell, J. K., and Dingwell, D. B. (2008). Viscosity of magmatic liquids: a model. *Earth Planet. Sci. Lett.* 271, 123–134. doi:10.1016/j.epsl.2008.03.038

Gualda, G. A. R., Ghiorso, M. S., Lemons, R. V., and Carley, T. L. (2012). Rhyolite-MELTS: a modified calibration of MELTS optimized for silica-rich, fluid-bearing magmatic systems. *J. Petrology* 53 (5), 875–890. doi:10.1093/petrology/egr080

Guillong, M., Meier, D. L., Allan, M. M., Heinrich, C. A., and Yardley, B. W. (2008). Appendix A6: SILLS: a MATLAB-based program for the reduction of laser ablation ICP-MS data of homogeneous materials and inclusions. *Mineralogical Assoc. Can. Short Course* 40, 328–333. https://ethz.ch/content/dam/ethz/special-interest/erdw/geopetro/mineralsystems-dam/documents/MAC_SC_40_Sills_description.pdf.

Gunnarsson, B., Marsh, B. D., and Taylor, H. P., Jr. (1998). Generation of Icelandic lavas from the Torfajökull central volcano: J. Volcan. *Geotherm. Res.* 83, 1–45. doi:10.1016/S0377-0273(98)00017-1

Hampton, R. L., Bindeman, I. N., Stern, R. A., Coble, M. A., and Rooyakkers, S. M. (2021). A microanalytical oxygen isotopic and U-Th geochronologic investigation of rhyolite petrogenesis at the Krafla Central volcano, Iceland. *J. Volcanol. Geotherm. Res.* 414, 107229. doi:10.1016/j.jvolgeores.2021.107229

Harrison, T. M., and Watson, E. B. (1983). Kinetics of zircon dissolution and zirconium diffusion in granitic melts of variable water content. *Contributions Mineralogy Petrology* 84, 66–72. doi:10.1007/BF01132331

Jochum, K. P., Stoll, B., Herwig, K., Willbold, M., Hofmann, A. W., Amini, M., et al. (2006). MPI-DING reference glasses for *in situ* microanalysis: new reference values for element concentrations and isotope ratios. *Geochem. Geophys. Geosyst.* 7, 1–44. doi:10.1029/2005GC001060

Jónasson, K. (1994). Rhyolite volcanism in the Krafa central volcano, north-east Iceland. *Bull. Volcanol.* 56, 516–528. doi:10.1007/BF00302832

Jónasson, K. (2007). Silicic volcanism in Iceland: composition and distribution within active volcanic zones. *J. Geodynam. V.* 43, 101–117. doi:10.1016/j.jog.2006.09.004

Kim, D., Brown, L. D., Árnason, K., Gudmundsson, Ó., Ágústsson, K., and Flóvenz, Ó. G. (2020). Magma "bright spots" mapped beneath Krafla, Iceland, using RVSP imaging of reflected waves from microearthquakes. *J. Volcanol. Geotherm. Res.* 391, 106365. doi:10.1016/j.jvolgeores.2018.04.022

Llovet, X., Pinard, P. T., Donovan, J. J., and Salvat, F. (2012). Secondary fluorescence in electron probe microanalysis of material couples. *J. Phys. D. Appl. Phys.* 45, 225301. doi:10.1088/0022-3727/45/22/225301

Masotta, M., Mollo, S., Nazzari, M., Tecchiato, V., Scarlato, P., Papale, P., et al. (2018). Crystallization and partial melting of rhyolite and felsite rocks at Krafla volcano: a comparative approach based on mineral and glass chemistry of natural and experimental products. *Chem. Geol.* 483, 603–618. doi:10.1016/j.chemgeo.2018.03.031

Mollo, S., Putirka, K., Iezzi, G., Del Gaudio, P., and Scarlato, P. (2011). Plagioclase–melt (dis)equilibrium due to cooling dynamics: implications for thermometry, barometry and hygrometry. *Lithos* 125, 221–235. doi:10.1016/j.lithos.2011.02.008

Nicholson, H., Condomines, M., Fitton, J. G., Fallick, A. E., Grönvold, K., and Rogers, G. (1991). Geochemical and isotopic evidence for crustal assimilation beneath Krafla. *Icel. J. Petrol.* 32, 1005–1020. doi:10.1093/petrology/32.5.1005

Paton, C., Hellstrom, J., Paul, B., Woodhead, J., and Hergt, J. (2011). Iolite: freeware for the visualisation and processing of mass spectrometric data. *J. Anal. Atomic Spectrom.* 26 (12), 2508–2518. doi:10.1039/C1JA10172B

Pope, E. C., Bird, D. K., and Arnórsson, S. (2013). Evolution of low-^{18}O Icelandic crust. *Earth Planet Sci. Lett.* 374, 47–59. doi:10.1016/j.epsl.2013.04.043

Rooyakkers, S. M., Stix, J., Berlo, K., Petrelli, M., Hampton, R. L., Barker, S. J., et al. (2022). Rifting and recharge as triggers of the mixed basalt–rhyolite Halarauður ignimbrite eruption (Krafla, Iceland). *Contrib. Mineral. Petrol* 177, 32. doi:10.1007/s00410-021-01881-7

Rooyakkers, S. M., Stix, J., Berlo, K., Petrelli, M., Hampton, R. L., Barker, S. J., et al. (2021). The origin of rhyolitic magmas at Krafla central volcano (Iceland). *J. Petrology* 62, egab064. doi:10.1093/petrology/egab064

Saubin, E., Kennedy, B., Tuffen, H., Nichols, A. R. L., Villeneuve, M., Bindeman, I., et al. (2020). Textural and geochemical window into the IDDP-1 rhyolitic melt, Krafla, Iceland, and its reaction to drilling. *GSA Bull.* 133, 1–16. doi:10.1130/B35598.1

Schmitt, A. K. (2011). Uranium series accessory crystal dating of magmatic processes. *Annu. Rev. Earth Planet. Sci.* 39, 321–349. doi:10.1146/annurev-earth-040610-133330

Shea, T., Hammer, J. E., Hellebrand, E., Mourey, A. J., Costa, F., First, E. C., et al. (2019). Phosphorus and aluminum zoning in olivine: contrasting behavior of two nominally incompatible trace elements. *Contrib. Mineral. Petrol* 174, 85. doi:10.1007/s00410-019-1618-y

Sigmarsson, O., Hémond, C., Condomines, M., Fourcade, S., and Oskarsson, N. (1991). Origin of silicic magma in Iceland revealed by Th isotopes. *Geology* 19, 621–624. doi:10.1130/0091-7613(1991)019<0621:OOSMII>2.3.CO;2

Simakin, A. G., and Bindeman, I. N. (2022). Convective melting and water behavior around magmatic-hydrothermal transition: numerical modeling with application to Krafla Volcano. *Icel. J. Petrology* 63 (8). doi:10.1093/petrology/egac074

Steiger, R. H., and Jäger, E. (1977). Subcommission on geochronology: convention on the use of decay constants in geo-and cosmochronology. *Earth Planet. Sci. Lett.* 36, 359–362. doi:10.1016/0012-821X(77)90060-7

Stern, R. A., and Amelin, Y. (2003). Assessment of errors in SIMS zircon U–Pb geochronology using a natural zircon standard and NIST SRM 610 glass. *Chem. Geol.* 197, 111–142. doi:10.1016/S0009-2541(02)00320-0

Torsvik, T. H., Amundsen, H. E. F., Trønnes, R. G., Doubrovine, P. V., Gaina, C., Kusznir, N. J., et al. (2015). Continental crust beneath southeast Iceland. *PNAS*, E1818–E1827. doi:10.1073/pnas.1423099112

Turner, J. S. (1979). *Buoyancy effects in fluids*. Cambridge University Press.

Vermeesch, P. (2018). IsoplotR: a free and open toolbox for geochronology. *Geosci. Front.* 9, 1479–1493. doi:10.1016/j.gsf.2018.04.001

Watson, E. B., and Harrison, T. M. (2005). Zircon thermometer reveals minimum melting conditions on earliest Earth. *Science* 308 (5723), 841–844. doi:10.1126/science.1110873

Zhang, Y., and Xu, Z. (2016). Zircon saturation and Zr diffusion in rhyolitic melts, and zircon growth geospeedometer. *Am. Mineralogist* 101, 1252–1267. doi:10.2138/am-2016-5462

Zierenberg, R. A., Schiffman, P., Barfod, G. H., Lesher, C. E., Marks, N., Lowenstein, J. B., et al. (2013). Composition and origin of rhyolite melt intersected by drilling in the Krafla geothermal field. *Icel. Contrib. Mineral. Petrol* 165, 327–347. doi:10.1007/s00410-012-0811-z